CHARACTERIZATION OF METAL FOAMS WITH SYNCHROTRON-TOMOGRAPHY AND 3D IMAGE ANALYSIS

A. Rack[1], A. Haibel[1], A. Bütow[2], B. Matijasevic[2] and J. Banhart[1,2]
[1] Hahn-Meitner-Institut Berlin, Germany; [2] Technical University, Berlin, Germany

Abstract: The design of porous metal structures is of high interest for novel lightweight industrial applications. Synchrotron tomography in combination with 3D image analysis is the suitable method to investigate these structures. In order to bring the foam production process from the laboratory to industrial scales a detailed knowledge of the control parameters' influence on the resulting pore structure is needed. We investigate metal foams made of aluminium and zinc. Our focus is set on early stages of the foam evolution prepared with blowing agents TiH_2 or ZrH_2 in different pre-treated conditions.

Introduction: Basic concepts for creating metallic foams have been developed during the 1950s [1] but could not be appropriately realized until ten years ago due to lack of technical abilities. Now, a broad spectrum of direct and indirect methods are used to create foams from different metals and metal alloys – e.g. the powder compact foaming process [2] , by using cast solid precursors [3] or by gas injection into the molten metal (air bubbling) [1]. With the increasing knowledge about the production of metallic foams the interest in them rises as well due to their high potential for novel lightweight applications [4]. The high specific stiffness in combination with their low weight strongly suggest to create load bearing elements out of aluminium foams for example in cars or planes in order to lower their energy consumption. Insulations or crash preventing elements are other important areas of application due to the high energy absorbing ability of metallic foams.

The key question is now how to produce metal foams in terms of serial application, e.g. for the car producing industry. Therefore, the influence of control parameters like the blowing agent, foamable material or foaming temperature on the resulting porous structure has to be known. Our non-destructive investigation method is the synchrotron tomography which has been proven in the past to be the suitable imaging method for foams, especially in early stages [5]. By varying the blowing agent parameters we create sample series in different expansion stages. The resulting 3D images from the synchrotron tomography are of high spatial resolution as well as with high element contrast. Therefore, we can have a closer look at the blowing agent inside of our samples and also at the micro-porosity. By using a 3D image analysis approach extended with methods derived from stochastic geometry [6] we are able to determine characteristics of the foam structure such as the critical thickness of cell walls, pore size distributions or spatial particle correlations.

Methods: The Hahn-Meitner-Institut Berlin (HMI) is maintaining a tomographical setup together with the Federal Institute of Materials Research and Testing, Germany (BAM) at the so-called BAMline located within BESSY II (Berlin electron storage ring company for synchrotron radiation, Germany) [7]. There, tomographic images with a spatial resolution of up to 3.6 μm can be obtained (higher resolutions down to 1.0 μm are being prepared). The X-ray energy can be varied from 6 to 60 keV with an energy resolution of 10^{-2}. The photon flux density is up to 10^{12} photons/mm^2/sec. For the aluminium foams we are working with 25 keV and for the zinc foams with 60 keV. Depending on the resolution used between 720 and 1800 radiographic images are taken in order to guarantee a good reconstruction.

Concerning the 3D image analysis we are working with a commercial software library called *a4iL* developed by the Fraunhofer Institute for Industrial Mathematics (ITWM Kaiserslautern, Germany) [8]. Optimized for speed and low memory consumption it is basically a tool-box consisting of such powerful functions as the erosion, dilation, Euclidean distance transformation, watershed transformation and so on. We are using these tools to build-up our own algorithms which have to be developed specifically for the investigated questions.

Our foam sample series are produced using the powder compact foaming process [2]. Pure zinc is mixed with 0.5 vol-% TiH_2 or ZrH_2 to make a foamable precursor. For the aluminium samples we are using an AlSiCu alloy mixed with 1.0 vol-% TiH_2 . By heating in a furnace including the possibility to measure exactly the temperature inside the samples, we create foams with different porosities P. The foaming process is interrupted by rapid cooling in order to have comparable samples in the same foaming stage but prepared with different parameters. For the blowing agent we are using sieved and non-sieved as well as pre-heat treated and as-received TiH_2 powder [9].
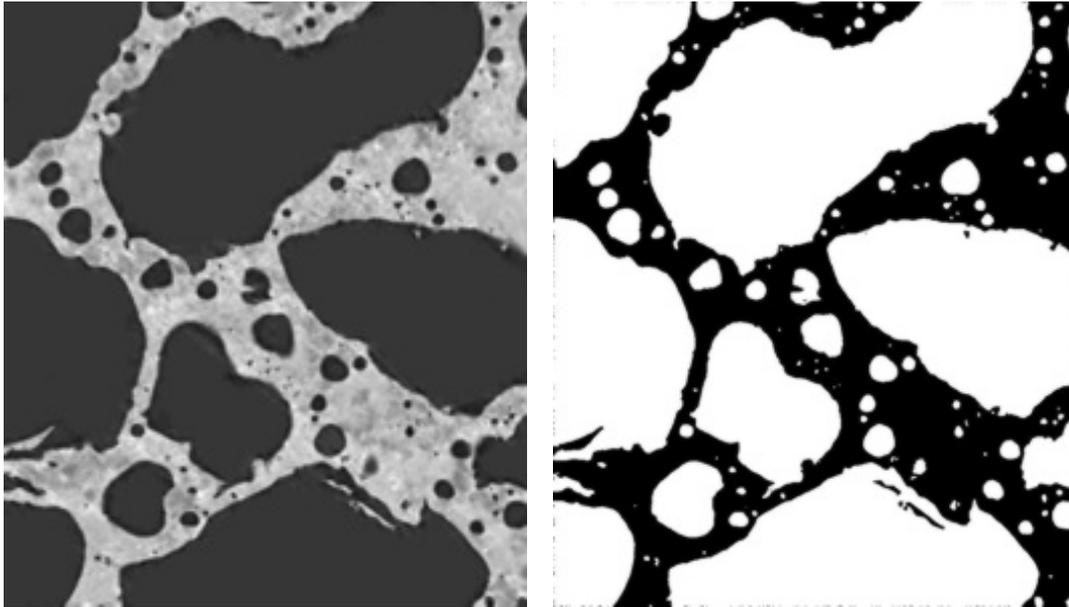

Fig. 1. Tomographic slice of an AlSiCu foam (left) with porosity P = 70% and corresponding Boolean image carrying only the pore information (right)

3D Image Analysis: The first step in order to evaluate three-dimensional images is the separation of morphological objects which are belonging to the same material or material phase (blowing agents, pores, metal matrix etc.). The left image in Fig. 1 shows as an example the gray-scaled tomographic slice of an AlSiCu foam. In order to separate for example the pores we are using a growth algorithm. Growth in this case means that in a first step all voxels (3D image points) with a gray value below a *threshold1* are set to Boolean value 1. These voxels are used in further steps as initial points where in successive stages all next neighbors of already marked pore volume with a gray value below a *threshold2* are denoted with Boolean value 1 as well. Voxels which have not been touched by the algorithm are set to Boolean value 0. The result is exemplarily viewable in Fig. 1, see right image. The complete pore information has been transformed into a Boolean image. All the remaining information has been skipped. The same algorithm can be applied for the blowing agent as well, only with different thresholds and growth direction.

These Boolean images can now be used to get statistical information like size distributions, shape characteristics or porosities. For the size distributions the image is labelled which means all voxels belonging to one topological object are tagged with an identification number. Plain counting of all voxels with the same identification number delivers the size of one object, if applied for the whole image the size distribution can be calculated [6]. The number of pore voxels divided by the number of all voxels within one image gives the porosity P.

Interesting questions are not only dealing with statistics – they go deeper into the structure of the object and, therefore, can not be answered straight forward as above. The usual morphological tools used here are erosion, dilation, Eulean number, watershed and Euclidean distance transformation. As we will heavily use the latter one within this paper the following paragraph is

focused on this transformation. The starting point of the Euclidean distance transformation is a Boolean image. For each foreground voxel (voxels with Boolean value 1) the minimal Euclidean distance to the background is calculated and the resulting value written at the voxels coordinates instead of the Boolean 1. The same is done vice versa for the background voxels but with the definition that all resulting minimal distances are negative in order to distinguish them from the foreground. One example is displayed in Fig. 2: Boolean image and Euclidean distance transformed image (sometimes also called distance map) [6].
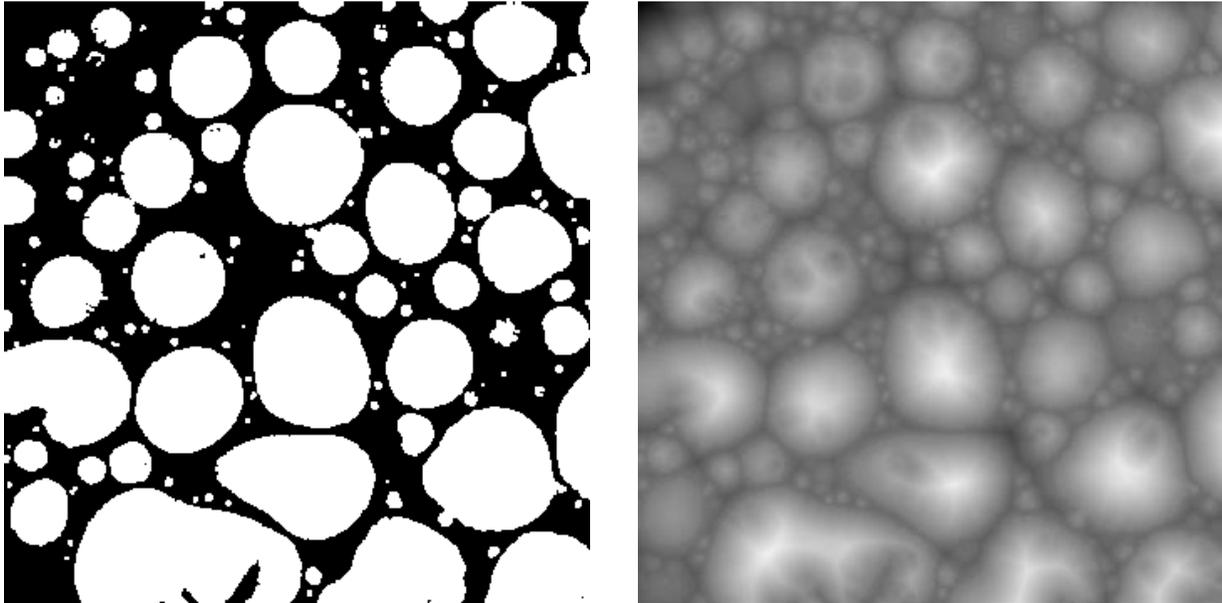

Fig. 2. Boolean image of a zinc foam's pore structure (left) with porosity P = 61% and corresponding Euclidean distance transformed (right)

One task we will have to deal with is the question if a spatial correlation does exist between the positions of blowing agents and the positions of pores inside a foam structure. An algorithm to investigate this has been developed by L. Helfen, J. Ohser et al. [10]. Based on successive dilation of the pore structure it calculates the density of foaming agent particles in identical pore neighborhoods. The latter are defined as difference between dilated and original image. The main disadvantages are the facts that the dilation can only be controlled by the size of the structuring element which is really a rough approach and that no characteristic information about the pore neighborhood is delivered. The Euclidean distance transform is the proper method to remove these disadvantages: inside a distance map all positive values are denoted as pores (see Fig. 2) and all remaining voxels with minimal absolute value are defining the first pore neighborhood in that structure. All voxels outside the pores and their first neighborhood with minimal absolute value are defining the next neighborhood and so on. By doing so, the pores can be dilated in small steps as well as extremely sensible to their shape and structure plus a characteristic value of the investigated volume fractions – the distance to the pores – is delivered. The foaming agent particle density found in each pore neighborhood is plotted against the distance to the pores. A decreasing density means that most of the foaming agents have been found close to the pores (correlation), vice versa we have anti-correlation and if the density is constant then the particles are scattered statistically in the investigated volume (see also Fig. 5).

Finally, we will take a look at the critical lamella thickness of foams. Here again we use the Euclidean distance transformation in order to dilate our Boolean pore structure. The basic idea of this algorithm is explained in Fig. 3. Inside the original Boolean pore image we have a fixed number of non-connected objects (left image in Fig. 3). Dilation means that the pore volume

increases and the background volume decreases. Therefore, sooner or later pores will touch each other which means, in the eyes of the algorithm, many objects are merging into one object (right image in Fig. 3). The algorithm dilates the pore structure step by step and calculates the number of objects after each dilation step. A plot of the number of objects versus the pore distances displays a significant drop at that distance where the minimum cell wall thickness is reached in terms of pore dilation.
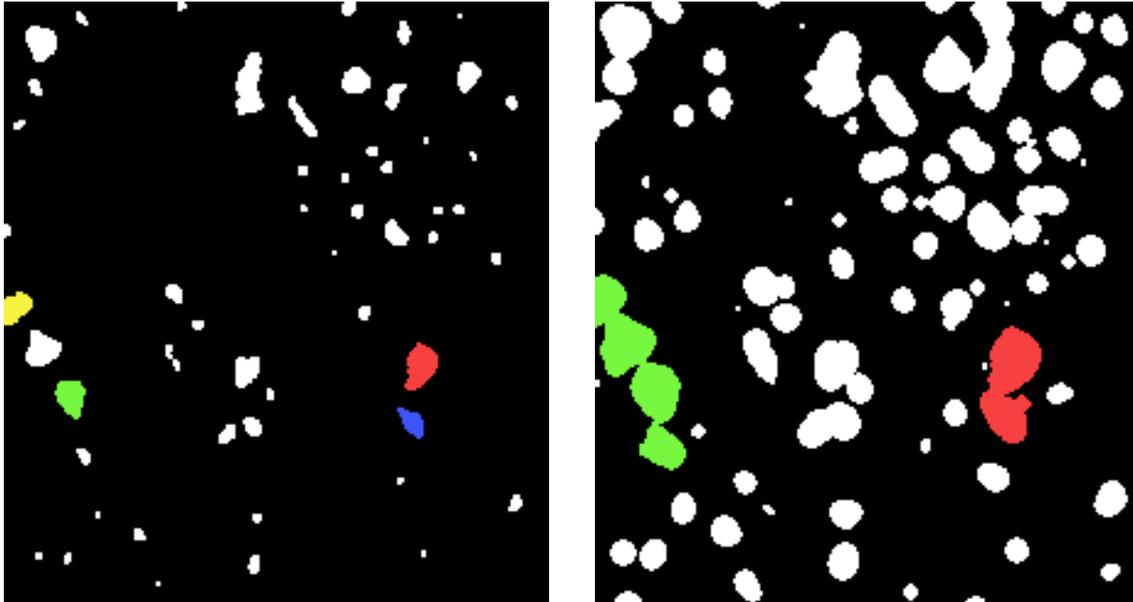
Fig. 3. Determining the minimum cell wall thickness: left image shows the original Boolean pore image (non-connected sample pores marked in different colors), right image displays the same image after ten dilation steps – the number of non-connected objects has decreased

Results: a) <u>Aluminium foam</u> – sample series have been created with AlSiCu. The foaming agent has been sieved so that we could use powders with mean particles sizes of below 20 μm, between 20 μm and 40 μm, between 40 μm and 80 μm and finally between 80 μm and 160 μm. Additionally, the foaming agent was heated for 180 minutes at 480 °C for some sample series. A detailed description of the sample preparation and the results concerning the foams statistic characteristics are discussed by A. Haibel et al. (see article "Quantitative analysis of pore-particle-correlations in metallic foams" in this proceeding book).

This article focuses on the critical cell wall thickness as well as on possible (anti-)correlations between the positions of foaming agents and the positions of pores inside the AlSiCu foam. Sample series in four extension stages have been prepared with different control parameters. The first two stages (non-foamed, ultra-short foamed) did not show any porosity in the tomographic images so we skip them for further investigations. Sample slices of the other two foaming stages (short foamed, long foamed) are displayed in Fig. 4. In case of the short foamed sample it is clearly visible that we have a lot of foaming agent (white areas – left image Fig. 4), the copper already formed an alloy with the aluminium (light-gray areas mainly around the pores – left image Fig. 4) and pores are starting to grow. In case of the long foamed sample (right image Fig. 4) one sees the bigger pores and that all the copper and nearly all foaming agents are decomposed. Other sample series show a similar behavior so we focused our investigations on the spatial correlations between the positions of foaming agents and the positions of pores on the short foamed samples.
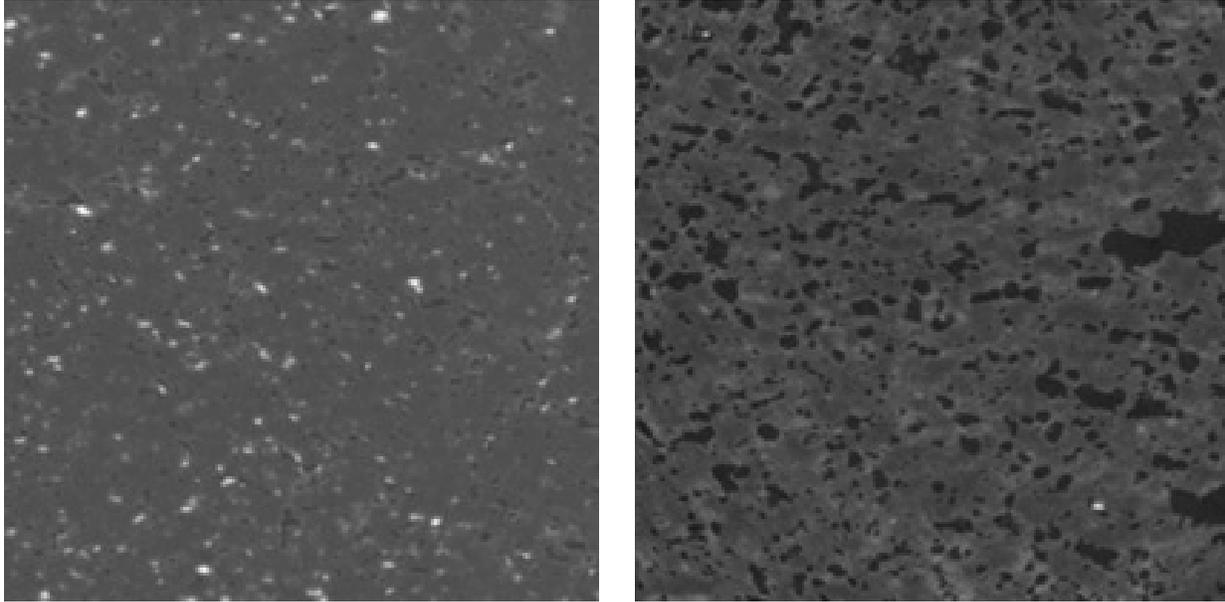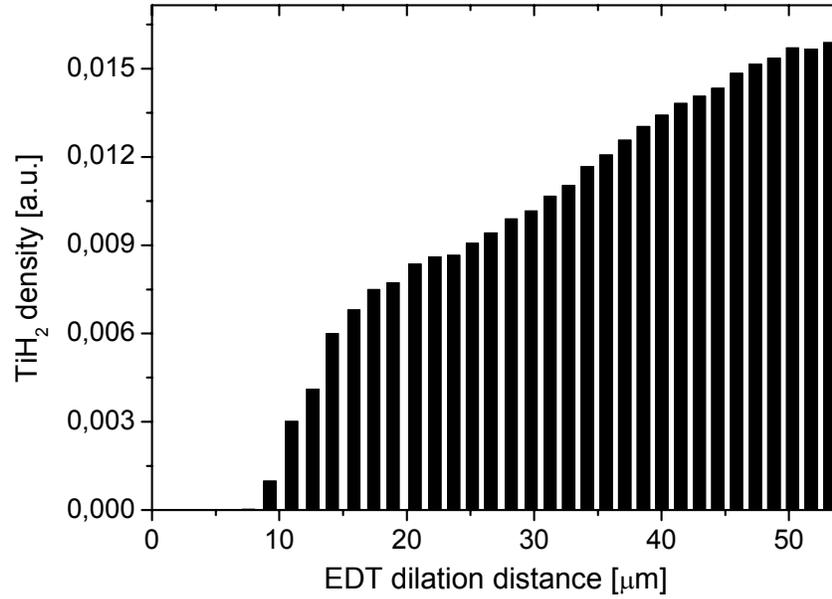
Fig. 4. AlSiCu foam with as-received foaming agent TiH$_2$ (mean particle size between 40 µm and 80 µm) in two extension stages: short foamed with porosity P=6% (left image, white – foaming agent, dark-gray – aluminium, light-gray aluminium-copper-alloy) and long foamed with porosity P=27% (right image, same color code as left)

The correlation algorithm was applied as described in the previous paragraph: the pore information and the foaming agents information is separated into two Boolean images. The Boolean pore image is dilated based on the Euclidean distance transformed image and in the resulting poor neighborhoods the density of TiH$_2$ particles is calculated. The algorithm terminates when the dilated pores have captured over 99% of the complete 3D image volume. An exemplarily plot of the particle density (arbitrary units) versus the dilation range in micrometer is displayed in Fig. 5.

The result is surprisingly enough an anti-correlation between the position of the TiH$_2$ particles and the pores inside the AlSiCu foam. This result is valid for all samples with as-received foaming agent in this expansion stage. For the sample series with treated TiH$_2$ only one tomographic image contains porosity and particles (the one with mean particle size of TiH$_2$ smaller 20 µm – for the rest there is either no porosity or the foaming agent is already decomposed) and here we have an anti-correlation as well. For complete results see Tab. 1. On a side note: in Fig. 4 left image an anti-correlation can already be estimated from the 2D slice but of course our results are reinforced by the investigation of the complete 3D volume.

Two types of pores are distinguished in the literature: type-I pores lie close to foaming agent particles because their gas release leads to a local pore formation; type-II pores are those with no blowing agents found in their adjacency. The latter are usually interpreted as cracks which happen due to hydrogen release before the foamable metal has reached its melting point [11]. Here, we found type-II pores which are clearly no cracks (compare Fig. 4) which points out that the nucleation of pores does not necessarily happen close to the blowing agent particles. Diffusion or channeling could be the answer how the gas migrates from the TiH$_2$ towards the nucleation centers and, therefore, the foaming process is more complicated as one would expect.

Fig. 5. Particle-pore-correlation function of AlSiCu foam with as-received foaming agent TiH$_2$ (mean particle size between 40 µm and 80 µm) – the positive gradient of the curve clearly indicates an anti-correlation between particle and pore position inside the investigated object

For all samples with a porosity P > 0 the algorithm to determine the minimum cell wall thickness was applied to the Boolean pore images as well. A complete listing of the results together with the control parameters is displayed in Tab. 1. The mean value of the critical lamella thickness is 25 µm with standard deviation of 4 µm and holds for all samples; even the porosity changes in orders of magnitude. This is also half of the value which has been known so far from other investigations [12].

foaming agent	TiH$_2$ mean particle size	foaming stage	porosity	correlation	minimal lamella thickness
pre-heat treated	< 20 µm	short foamed	5%	anti	33 µm
pre-heat treated	< 20 µm	long foamed	70%	—	27 µm
pre-heat treated	20 µm – 40 µm	short foamed	19%	—	29 µm
pre-heat treated	20 µm – 40 µm	long foamed	64%	—	27 µm
pre-heat treated	40 µm – 80 µm	short foamed	12%	—	27 µm
pre-heat treated	40 µm – 80 µm	long foamed	64%	—	26 µm
pre-heat treated	as-received	short foamed	14%	—	22 µm
pre-heat treated	as-received	long foamed	50%	—	21 µm
as-received	20 µm – 40 µm	short foamed	12%	anti	22 µm
as-received	20 µm – 40 µm	long foamed	46%	—	26 µm

as-received	40 µm – 80 µm	short foamed	6%	anti	25 µm
as-received	40 µm – 80 µm	long foamed	27%	—	20 µm
as-received	80 µm – 160 µm	short foamed	2%	anti	30 µm
as-received	80 µm – 160 µm	long foamed	33%	—	20 µm
as-received	as-received	short foamed	9%	anti	25 µm
as-received	as-received	long foamed	14%	—	25 µm

Table 1: Control parameters and results of the investigation on AlSiCu foam samples

b) <u>Zinc foam</u> – sample series have been created with pure zinc and TiH_2 or ZrH_2 as foaming agent. Again the foaming agent was sieved so we had powders with mean particles sizes above or below 28 µm for use. The zinc foams investigated here are in an extended expansion stage (high porosity). Two sample slices of the investigated zinc foams are displayed in Fig. 6.
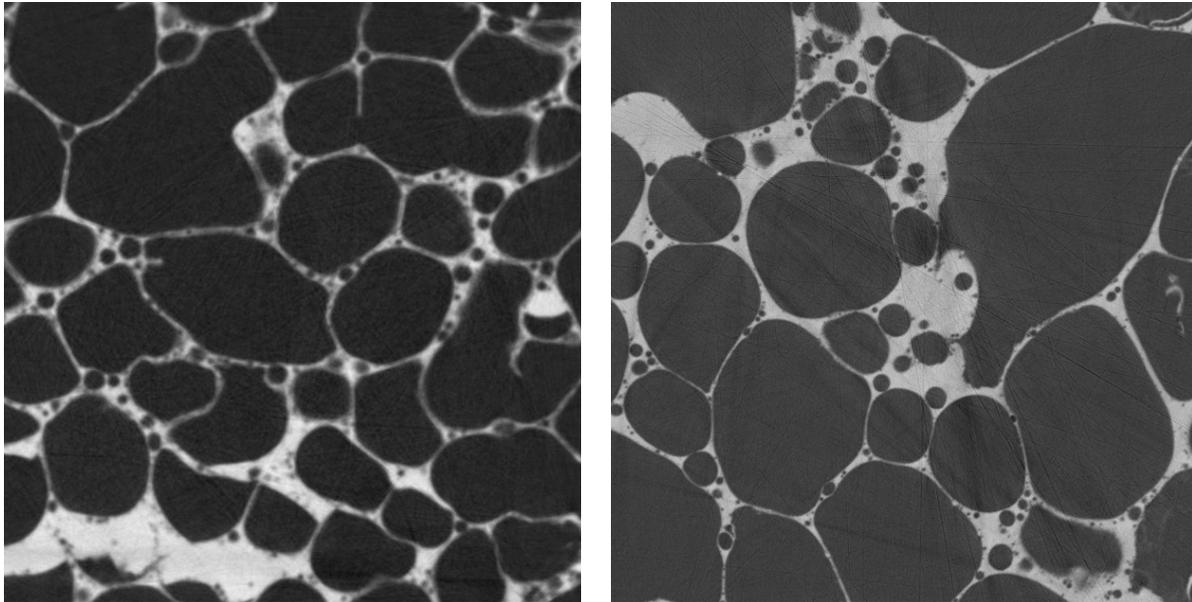
Fig. 6. Zinc foam with as-received blowing agents in extended foaming stage: TiH_2 (mean particle size below 28 µm) with porosity P=75% (left image, white – zinc) and ZrH_2 (as-received) with porosity P=79% (right image, same color code as left), foaming agents are already decomposed

The critical cell wall thickness of zinc foams has already been investigated with the help of synchrotron tomography. At that time the minimum lamella thickness was measured with the help of a commercial rendering tool on 2D slices [13]. Here, we present for the first time investigations in real 3D. The applied algorithm to determine the critical cell wall thickness is the same as in previous chapters: tomographic images of the prepared samples were taken, Boolean pore images created and the algorithm applied. The results are displayed in Tab. 2. The mean value of the critical lamella thickness is 26 µm with a standard deviation of 5 µm.

foaming agent	foaming agent mean particle size	foaming stage	porosity	minimal lamella thickness
ZrH_2	as-received	extended foamed	79%	19 µm

TiH$_2$	> 28 μm	long foamed	68%	23 μm
TiH$_2$	< 28 μm	extended foamed	75%	30 μm
TiH$_2$	> 28 μm	long foamed	72%	31 μm

Table 2: Control parameters and results of the investigation on Zn foam samples

Conclusions: Our 3D image analysis of tomographic images showing AlSiCu foam in identical foaming stages but with blowing agents differently prepared are displaying a clear anti-correlation between the position of the pores and the agent particles inside the foam structure (see also Tab. 1). These type-II pores are usually interpreted as cracks or to happen at triple grain junctions in polycrystalline zinc [11]. The diffusion velocity of hydrogen in liquid aluminium is very high [14]. Therefore, a similar effect like in polycrystalline zinc can be imagined as well.

The results for the critical lamella thicknesses in zinc as well as aluminium foams (see Tab. 1 and Tab. 2) are by a factor of two smaller than the one reported in previous investigations [12, 13]. The reason is quite obviously the fact that those investigations were done in a 2D approach – therefore, the results can only be an interpreted estimate as they neglect the real 3D nature of this problem. Here, we present results based on a real three-dimensional investigation.

The critical cell wall thicknesses for aluminium foams and zinc foams are in the same size range (25 μm with standard deviation of 4 μm for AlSiCu, 26 μm with standard deviation of 5 μm for Zn). As reported in [13] the viscosity for aluminium at its melting point (660 °C) is η_{melt}=1.25 mN/m^{2}s, three times smaller than for zinc (3.75 mN/m^{2}s) at its melting point (419 °C) [15]. This supports the conclusion that the viscosity close to the melting point of the foamable metal or metal alloy does not have very much influence on the resulting foam stability displayed via the critical lamella thicknesses. This is in agreement with previous observations [16].

References:

[1] M. Ashby, A. Evans, N. Fleck, L. Gibson, J. Hutchinson, H. Wadley, *Metal Foams: A Design Guide*, Butterworth-Heinemann (2000)

[2] J. Banhart, *Progress in Materials Science* 46, 559-632 (2001)

[3] V. Gergely, B. Clyne, *Advanced Engineering Materials* 2, 175-178 (2000)

[4] J. Banhart, N.A. Fleck, A. Mortensen, eds., *Cellular Metals: Manufacture, Properties, Applications*, MIT-Verlag Berlin (2003)

[5] L. Helfen, T. Baumbach, H. Stanzick, J. Banhart, A. Elmoutaouakkil and P. Cloetens, *Advanced Engineering Materials* 4, 808-813 (2002)

[6] J. Ohser and F. Mücklich, *Statistical Analysis of Microstructures in Materials Science*, John Wiley & Sons (2000)

[7] G. Weidemann, J. Goebbels, Th. Wolk, H. Riesemeier, *BESSY Annual Report 2001*, CD-ROM & WWW, 249-250, Project-No.: 0103-I-0017 (2001)

[8] http://www.itwm.fhg.de/mab/projects/a4iL

[9] B. Matijasevic, S. Fiechter, I. Zizak, O. Görke, N. Wanderka, P. Schubert-Bischoff, J. Banhart, *Decomposition behaviour of as-received and oxidized TiH$_2$ powder*, Powder Metallurgy World Congress, conference book (2004)

[10] L. Helfen, H. Stanzick, J. Ohser, K. Schladitz, P. Pernot, J. Banhart and T. Baumbach, proceeding of the SPIE SS/NDE conference (2003)

[11] L. Helfen, *Investigation of the Structure, Formation and Properties of Porous, Cellular and Low-Density Materials with Synchrotron-Radiation Imaging*, PhD thesis University Saarland, Germany (2003)

[12] H. Stanzick, M. Wichmann, J. Weise, L. Helfen, T. Baumbach and J. Banhart, *Advanced Engineering Materials* 4, 814-823 (2002)

[13] A. Rack, A. Haibel, B. Matijasevic, J. Banhart, *Synchrotron tomography on zinc and aluminium foams*, Cellular Metals: Manufacture, Properties, Applications (MetFoam 2003), conference book, MIT-Verlag, Berlin, 295-300 (2003)

[14] C. Körner, M. Thies, F. Singer, *Advanced Engineering Materials* 10, 765-769 (2002)

[15] C. J. Smithells, E. A. Brandes, *Metals Reference Book*, Butterworth London & Boston (1976)

[16] T. Wübben, H. Stanzick, J. Banhart, S. Odenbach, *Journal of Physics: Condensed Matter* 15, 427-433 (2003)